Journal of Applied Electrochemistry **30**: 767–775, 2000.

An experimental investigation of bubble-induced free convection in a small electrochemical cell

P. BOISSONNEAU and P. BYRNE*
Faxén Laboratory, Applied Electrochemistry, Royal Institute of Technology (KTH), Teknikringen 42, SE-100 44 Stockholm, Sweden
*(*author for correspondence, fax: +46 8 10 80 87, e-mail: phil@ket.kth.se)*

Received 24 September 1999; accepted in revised form 29 February 2000

Key words: bubble evolution, gas evolution, hydrodynamics, hydrogen gas, LDV

Abstract

The sodium chlorate production process is run in large electrolysers where electrolyte flows between the electrodes due to the natural convection from hydrogen gas evolution. A brief review is given of electrolytic gas generation at electrode surfaces and of previous studies. A small, enclosed rectangular cell was used to electrolyse both a Na_2SO_4 and a $NaCl/NaClO_3$ solution, in order to produce hydrogen and oxygen bubbles at one or both of the electrodes. The two-phase flow regimes, bubble sizes, gas fraction and fluid velocities between the electrodes were investigated using microscope enhanced visualisation, laser doppler velocimetry and particle image velocimetry. The practicality of each of the measuring methods is analysed and it is concluded that laser doppler velocimetry is the most robust method for measuring such systems. The experimental results are discussed and conclusions are drawn relating gas evolution to the hydrodynamics of electrolyte flowing through a narrow vertical channel. The major conclusions are that fluid flow in systems with bubble evolution can transform from a laminar to a turbulent behaviour, throughout the length of the cell, and that both turbulence and laminar behaviour can exist across the cell channel at the same horizontal plane.

List of symbols

n	index depending on gas fraction
Q_g	gas flow rate ($m^3\,s^{-1}$)
Q_l	liquid flow rate ($m^3\,s^{-1}$)
U_b	bubble velocity ($m\,s^{-1}$)
U_l	liquid velocity ($m\,s^{-1}$)
U_r	relative velocity between the two phases ($m\,s^{-1}$)
U_∞	rising velocity of a single bubble in a stagnant fluid ($m\,s^{-1}$)
u'	turbulent intensity ($m\,s^{-1}$)
β	volumetric flow gas fraction

1. Introduction

Major achievements concerning the study of the hydrodynamics of electrochemically evolved gases have occured during the past thirty years [1]. Electrolytically evolved bubbles can be produced at either one or both electrode surfaces. Their presence can be detrimental to the process by blocking the electrode of active area or causing added resistance in the electrolyte.

Most industrial electrochemical processes are intrisincally related to mass transfer, which has led to an increase in investigations of the relationship between electrochemistry and hydrodynamics. Electrochemical reactions can be strongly influenced by pump-induced electrolyte flow, through an increase in a participating species' mass transfer to an electrode surface. Alternatively, flow and mass transfer can be imposed by electrochemically producing bubbles at an electrode surface. This is relevant within the chlorate process, where hydrogen bubbles produced at the cathode lead to flow in the channel.

2. Bubble production

2.1. *Chlorate process*

Sodium chlorate ($NaClO_3$) is mostly used in the paper industry as a base chemical in paper bleaching. Its production starts with the electrochemical oxidation of chloride ions and reduction of water from a sodium chloride solution (NaCl). Hydrogen gas is produced at the cathode and remains as gas bubbles in the system. Chlorine is produced at the anode, but almost immediately disappears through reacting with other species in the electrolyte. The oxygen gas bubble, an unwanted byproduct, is also produced at the anode and robs the system of 2–4% of the current [2].

The industrial production of sodium chlorate occurs in large vessels containing hundreds of cells (anode–cathode pairs). Above these banks of cells, 'chimneys' are constructed that gather the hydrogen gas and generate velocities in the cell channels that can reach anything between 0.1 and 2 m s^{-1}.

Numerical models have previously been developed for this process by several authors. These models relate mass transfer of the relevant species, involved in the reactions at the electrode surfaces, to electrolyte single phase flow in the channel. Byrne et al. [2] imposed a fixed velocity on the electrolyte at the entrance of the channel, which developed into a parabolic Poiseuille profile. Alternative models have assumed that flow is already a developed phenomenon within the channel, and that simplified diffusion equations, using size-averaged diffusion layers, describe the mass transfer to electrodes [3, 4]. It is therefore appropriate for experimental investigations to adequately describe the hydrodynamics of this and similar systems.

The majority of experimental work on bubble behaviour in vertical channels, which has led to the development of several models, has been carried out with injected gases sparged through porous media at the bottom of a channel. The model of Bankoff [5] assumed that bubble velocity is equal to that of its surrounding liquid, and described the velocity profile in the shape of a two-dimensional power law expression. The drift flux model of Zuber and Finlay [6] considered local relative drift velocities between bubbles and the surrounding liquid. Others have shown that gas concentration and bubble distributions depend upon gas fractions, fluid velocities and on channel geometries [7–10]. All of these models are macroscopic in nature and do not consider the local effects that bubbles have on their surrounding system.

2.2. *Gas evolution and coalescence*

Electrolytically evolved bubbles are produced at the electrodes in the dissolved state. Small nuclei of bubbles start at imperfections in the electrode surface and are subsequently fed from the highly supersaturated, surrounding electrolyte [11, 12]. Grown bubbles leave the electrode surface depending on the surface conditions, angle of contact between the bubble and surface and macroconvective properties of the electrolyte. The released bubble continues to take in gaseous species from the surrounding electrolyte, growing in size as it rises through the channel.

The conditions of the system and properties of both the bubbles and electrolyte determines the extent of coalescence [13, 14]. Bubbles collide and entrap a thin film of fluid between them which, in turn, drains until it is too thin to resist the forces of attraction and the two bubbles rupture to form one. Collisions can occur through three mechanisms [15]. The most predominant of these results from the nature of turbulence, where bubbles, travelling in one vector, collide with bubbles travelling in alternative vectors. The appropriate velocity for a bubble to coalesce is determined to be the turbulent eddy velocity with a length scale of bubble-size order. Coalescence has a significant effect on mass transfer and the electrochemical properties of the system [16].

Hydrogen evolution can instigate turbulence and has a pronounced effect on the mass transfer to both electrodes. Its production and behaviour in electrolyte flow has been of interest for the past thirty years [17–19]. The majority of industrial cathodes produce hydrogen bubbles with mean diameters of about 50 μm [20] to 200 μm [21, 22]. Janssen et al. [16] defined a hybrid model where hydrogen bubble evolution follows two different mechanisms. The first involves a single bubble detaching from the electrode surface, which stays confined to the bubble layer and continues to grow while diffusing slowly towards the bulk. The second mechanism involves a bubble on the surface coalescing with other bubbles in its vicinity, resulting in the subsequent bubble jumping directly into the bulk region.

2.3. *Cell hydrodynamics*

The sizes and physical properties of bubbles evolved in electrochemical systems depend upon the nature of the electrolyte and the electrode materials [22, 23]. The type of bubble generation has a profound influence on the hydrodynamics of the surrounding electrolyte, which has led to the development of three basic models [1]. The penetration effect [24] says that a detached bubble transfers a mixing momentum to the electrolyte, during its rise, as if it had created a wake. The microconvection effect [25] says that the growth of a bubble on the surface pushes liquid in all directions along the electrode surface. The effect amounts to localised laminar flow in the vicinity of nucleation sites with the subsequent effect that this convection has on mass transfer. Finally, the hydrodynamic or macroconvective effect was suggested, which said that the macroflow, induced by the rising of swarms of bubbles, is responsible for the increase in mass transfer to the respective electrodes [26]. Fukunaka et al. [27] ran experiments on a sectioned electrode where gas was evolved from the opposite electrode. They noticed that the mass transfer coefficient increased with increasing current density, but that there were also two areas of behaviour. These were attributed to laminar behaviour, occurring at low current densities, and turbulent behaviour at higher current densities.

Previous investigations have experimentally looked at gas evolution in narrow channels between vertical electrodes, and in conditions corresponding to industrial processes [28–32]. This investigation has measured the two-phase flow in a small cell composed of two flat-plate electrodes placed in a stagnant solution. Bubble sizes, velocity profiles between the electrodes and gas fraction have been determined, through microscope enhanced visualization, laser doppler velocimetry (LDV) and particle image velocimetry (PIV).

3. Experiments

The experiments were run on a small, vertical cell made of plexiglass, 12 cm long and 3 cm wide, in which the two plate electrodes, 4 cm × 3 cm, were embedded, as shown in Figure 1. The width of the channel between the electrodes, or the 'cell gap', was set to 3 mm. The initial length of the channel, where no gas evolution was to occur, was included so as to allow the measurement of flow profiles without the interference of bubbles, whilst the top part of the channel was where the final bubble concentration could be measured. Two thin glass plates were placed on the sides of the plexiglass walls in order to enclose the channel and force the electrolyte to enter from beneath.

The trials were run at room temperature. The cell sat in five litres of Na_2SO_4 (50 g l^{-1}) solution, for the investigation of water splitting, and in a NaCl (50 g l^{-1})/$NaClO_3$ (200 g l^{-1}) solution when investigating chlorine/chlorate production. Electrolysis of the Na_2SO_4 electrolyte gave both hydrogen and oxygen evolution, with approximately 100% current efficiencies. The electrolysis of the NaCl (50 g l^{-1})/$NaClO_3$ (200 g l^{-1}) electrolyte produced hydrogen and chlorine, where the chlorine reacted rapidly, and was not noticeable as bubbles. Oxygen was produced in this electrolyte as a byproduct and amounted to approximately 2–4% of the anode current. Hydrogen was produced on a coated titanium cathode in both systems, whilst two types of DSA® electrode, coated respectively with chlorine and oxygen evolving electrocatalysts, were used as anodes.

3.1. *Measurement methods*

The system was studied using microscope enhanced visualisation, in order to determine bubble sizes and concentrations, LDV, which enabled measurements of the velocity profiles in the channel, and PIV, which visualized the global behaviour of the two phase flow.

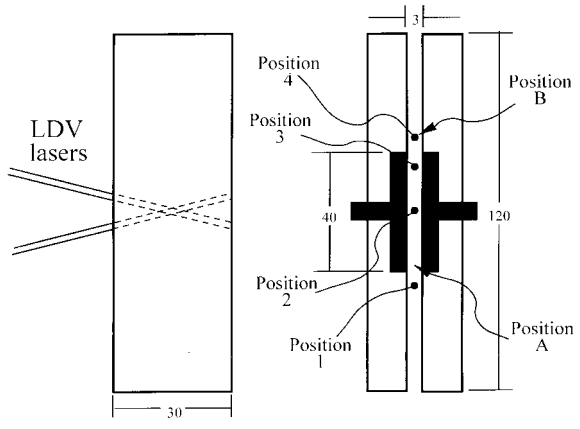

Fig. 1. Cell dimensions, LDV arrangement and positions for the visualization trials (positions A and B) and for the LDV trials (positions 1–4).

3.1.1. *Microscope enhanced visualisation*

Microscope enhanced visualisation enabled us to take images and view the two-phase flow in different positions along the channel height. The arrangement involved a captor coupled device (CCD) video camera connected to a microscope on the front side of the cell, and lighting provided from behind. The video camera was fairly standard and contained a 6.4 mm × 4.8 mm CCD cell composed of 542 × 542 pixels. Images, consisting of two interlaced frames, were acquired at 50 Hz, and the microscope offered a magnification of up to 40×. The lighting arrangement consisted of a white light source of 150 W, which could be run constantly or stroboscopically, and it was focused by a convergent lens into the region of the measurement volume through a method similar to Boissonneau [33].

To measure bubble sizes and concentrations, a bubble counting method was used. The continuous light source could be used at very low bubble velocities, where the flow could virtually be 'frozen' by the video camera shutter opening time of 0.02 s. Alternatively, still images could also be provided using stroboscopic light, pulsed at the same frequency as the video camera. The images were digitised by the CCD and loaded into a Macintosh Power PC Quadra 650 via a Scion LG3 frame-grabber card controlled by the NIH Scion Image 1.62 software package. Two vertical positions along the cathode were investigated. Position A corresponded to a position at the bottom of the electrodes, where bubble evolution had just started. Position B was chosen to be just above the electrodes, in a region where the hydrogen bubbles had already been produced and were not affected by an evolving environment near the electrodes.

Images were taken at three current densities: $j = 500$, 1000 and 2000 A m^{-2} in the 50 g l^{-1} Na_2SO_4 solution. Sixty pictures were taken in each position and at each current density.

3.1.2. *Laser doppler velocimetry*

Bubble and fluid velocities were measured in the channel using laser doppler velocimetry (LDV), at different heights along the length of the cell, in order to determine the evolution of the flow velocity profile. Position 1 was 5 mm below the electrodes, position 2 was at the middle position of the electrodes, position 3 was 5 mm from the top of the electrodes, and position 4 was 5 mm above the electrodes.

A Spectra Physics argon laser source, model 2080, with an output power of 30 W was used as the laser probe. The Aerometrics LDV instrument separated green light (514 nm) from blue (488 nm) and enabled a two component velocity measurement. The measurement volume was an ellipsoid of 80 μm in width and 200 μm in length and was made up of an interference pattern of light and dark fringes. The emitter and receiver were situated in a position at the front of the cell and backscattered light was collected and focused onto a photomultiplier. This backscattered arrangement is

unusual, in bubbly flow measurements as the majority of the light scatters in the forward direction [34]. The arrangement was chosen due to the fact that the cell involved a narrow but relatively deep channel, which did not offer adequate space for the light to pass to the photomultiplier in a forward-scattered arrangement. The experimental arrangement is illustrated in Figure 1.

Bubble velocity was measured in the bubble layer and in the bulk. Not all the gas was liberated from solution and there remained a sufficient amount of recirculating bubbles, mostly of diameters less than 10 μm, which enabled fluid velocity measurements in the centre of the channel. Velocity profiles were mapped at each of the positions for the two electrolytes at three current densities; $j = 500$, 1000 and 2000 A m^{-2}. Measurements were recorded upon the acquisition of 4000 validated samples.

3.1.3. *Particle image velocimetry*

Particle image velocimetry (PIV) was also used to investigate the system, particularly with respect to finding the point where laminar flow transferred to turbulence. The camera was placed perpendicular to a laser sheet, being shone from below, which crossed the channel perpendicular to the electrodes. The Dantec PIV equipment composed of two Yag lasers with a maximum power of 400 mJ pulse^{-1}, which were set-up to align the two beams on the same axis and guarantee a wave length of 532 nm. An optic head, enabling a sheet thickness from 200 μm to several millimetres, formed the laser sheet. The camera was a Kodak Megaplus (Model Es 1.0), and the optic control, a Nikon 60, gave image sizes of 1 cm $\times$ 1 cm. The cell was run at the one current density and, once the flow appeared to be steady, the camera was placed successively at 1 cm intervals so as to achieve a picture of the total height of the electrode.

4. Results and discussion

4.1. *Bubble sizes*

Visualisation trials were useful in achieving a qualitative view of the system. The image at position A showed that the bubbles stayed confined to the electrode, where the majority of the bubbles were seen to adhere along it. The bubble layer was thicker in the region at the top of this first image, where the thickness could be measured as equalling the mean bubble diameter. Bubbles were still seen to be very concentrated close to the wall, at position B, although two further regions were noticeable. It is postulated that there exists an adherence region, where the bubbles are stuck to or are very close to the electrode surface, which has a thickness the size of the mean bubble diameter. The second region appeared as a grey cloud in the image, and was very bubble concentrated. Discernible bubbles, in this region at position B, were twice as large as those seen in the image of position A, showing that bubbles also grow in the bubble diffusion region [12].

The third region contained quite dispersed bubbles, which had arrived there through bursts from the cathode surface into the electrolyte. This region is deemed to have a supersaturation at or near the level of that of the bulk solution, as bubbles in this region do not increase significantly in size throughout the length of the cell. The bubble bursts occurred sporadically and were composed mostly of large bubbles. It is deemed that it was basically the mechanism of coalescence, described by Janssen et al. [16], which was observed here. They defined a hybrid model where hydrogen bubble evolution follows two different mechanisms, the second of which involves a bubble on the surface coalescing with other bubbles in its vicinity, resulting in the subsequent bigger bubble jumping directly out of the adherence region and into the bulk region. The different parts of the bubble layer are shown in Figure 2.

Analysis of the images was achieved through a semi-automatic treatment contained in the software. The treatment managed to accurately account for the bubbles, located in the region fed by jumping-bubble bursts, but not in the bubble diffusion or adherence regions. The bubbles in the third region were deemed to have reached their final size and they were measured and counted at position B at a current density of 1000 A m^{-2}. The bubble distribution is shown in Figure 3. Bubbles of a size less than 45 μm were too hard to ascertain and were excluded from the distribution. Extrapolation of the results shows that there would not have been too many bubbles in this order of size. As the bubbles that entered this third region are basically bubbles that have coalesced, and the bubbles that they have taken with them when they 'jumped' from the electrode surface, an accurate size distribution is not given in this Figure. Nevertheless, it is assumed that the bubble size distribution (Figure 3) is qualitatively consistent, between the respective current densities and electrode materials, and that this type of visualization is useful in qualifying bubble sizes, from evolution (position A) to their final size (position B).

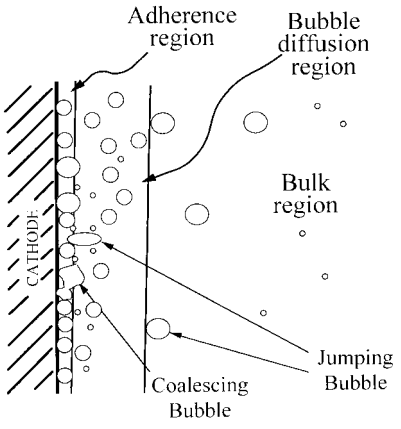

Fig. 2. Definition of the zones in the bubble layer beside the electrode.

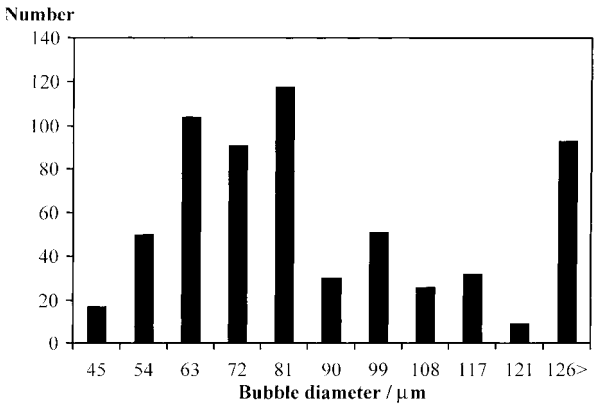

Fig. 3. Bubble size distribution at position B where $j = 2000$ A m^{-2} in a Na_2SO_4 (50 g l^{-1}) electrolyte.

Figure 4 shows the mean hydrogen bubble diameter versus current density for the two positions on a titanium cathode, a roughened stainless steel cathode, and results from Glas et al. [21]. They evolved hydrogen on a flat-plate platinum cathode, sitting freely in a stagnant solution where turbulence would not be present. They calculated empirically that bubble radius is proportional to the diffusivity of the participating ions in solution, the time of bubble growth, and current density raised to the power of 0.55. The experimentally observed bubble diameters were mostly smaller than those which would be found using their formula. Vogt [12] found that the presence of stirring diminished the average size of a detached bubble, due to the fact that an increase in macrovection decreases the microconvective effects that feed the growth of a bubble. Macroconvection also 'steepens' the concentration gradient from the electrode surface to the bulk, providing a smaller region of highly concentrated, dissolved gas with which to feed the growing bubble. Therefore, an expression that would predict bubble size from the parameters of a system would have to take into account not only bulk concentration, diffusivity and current density, but also the hydrodynamic and material properties of that system.

4.2. *Velocity profiles*

LDV measurements were impossible in the adherence region of the bubble layer because of the high bubble concentrations. In this region, the bubbles could not be located independently from each other and the measurement volume sent back very noisy signals. Measurements at first became accurate at between 200 μm and 300 μm from the electrode surfaces, depending on current density and the vertical position.

Results from the LDV measurements were divisible into two parts and the bubble diffusion boundary of the bubble layer could be qualitatively proved to exist by observing the time it took acquiring these measurements. About 60 s was required for measuring flow in the second region of the bubble layer, as opposed to more than 100 s past this boundary and in the region of the bulk. This was because the large number of bubbles in the bubble layer gave quicker measurement resolutions, whereas only a few recirculating bubbles were available for measurement outside of this boundary. Despite the fact that fluctuations occurred to the bubble layer boundary, especially when bursts of bubbles were ejected from the surface, its presence was quite distinct and it was deemed appropriate that the boundary layer thickness could be estimated in this way.

Velocity profiles, from the electrolysis of sodium sulphate, are shown in Figures 5, 6, 7 and 8, where the anode is on the left-hand side and the cathode on the right-hand side of the graphs. In position 1 (Figure 5), before gas evolution enters the system, the velocity profiles were almost symmetrical and are compared to the shape of the Poiseuille power law profile at conditions of $j = 2000$ A m^{-2}. This Figure shows that the measured velocities were fairly well aligned with this curve, in the centre of the channel, yet deviated away from the theoretical curve in the region of the walls. This is due to acceleration in the system being localised to where the bubbles evolved, and not uniform over the channel width.

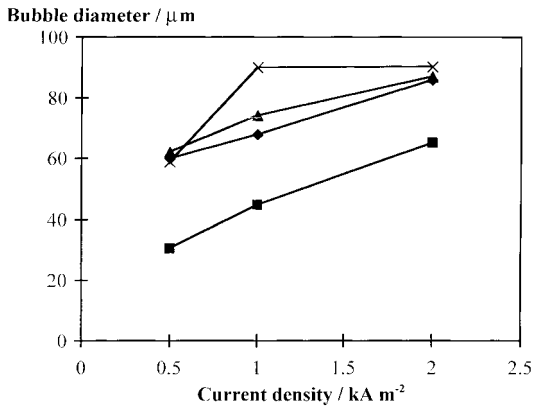

Fig. 4. The mean hydrogen bubble diameter versus current density, at position A, on the titanium electrode (■), position B, on the titanium cathode (▲), a roughened stainless steel cathode (×), and from the results of Glas et al. [21] (◆).

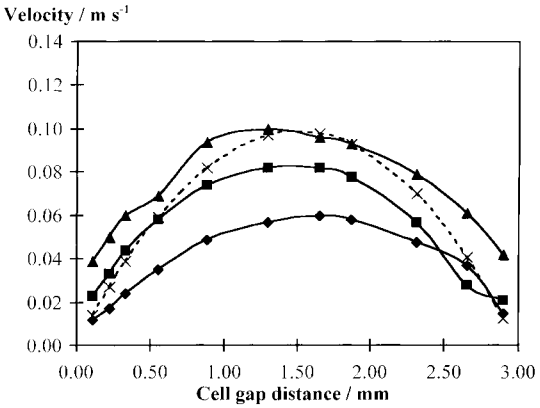

Fig. 5. Velocity profiles at the beginning of the channel, position 1, for the three current densities: $j = 500$ (◆), 1000 (■), 2000 (▲) A m^{-2}, in a Na_2SO_4 (50 g l^{-1}) electrolyte. The Poiseuille power law, at the condition of $j = 2000$ A m^{-2}, is given as a comparison (×).

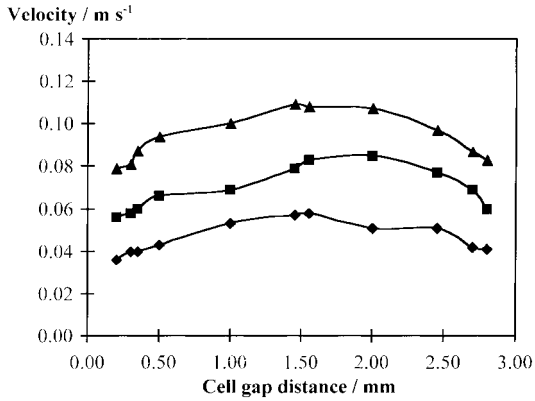

Fig. 6. Velocity profiles in the middle of the channel, position 2, for the three current densities: $j = 500$ (◆), 1000 (■), 2000 (▲) A m^{-2}, in a Na_2SO_4 (50 g l^{-1}) electrolyte.

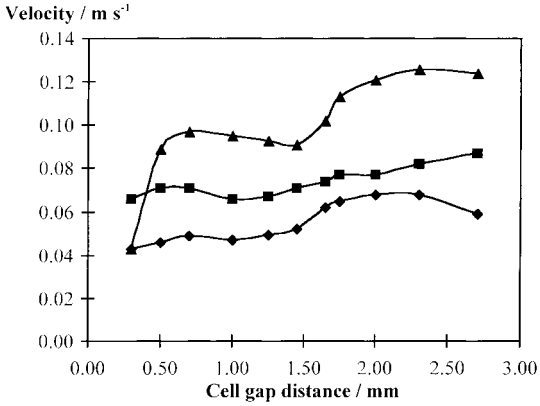

Fig. 8. Velocity profiles above the electrodes, position 4, for the three current densities: $j = 500$ (◆), 1000 (■), 2000 (▲) A m^{-2}, in a Na_2SO_4 (50 g l^{-1}) electrolyte.

Figure 6 shows the velocity profiles at position 2, which are flatter than at position 1, due to the effect that bubbles have upon entering the system. The bubble layers were still relatively thin at this position, and most of the bubbles were present in the bubble diffusion region of the bubble layer. Progressing up the length of the channel, the greater effect that evolved bubbles have on free convection can be seen in Figures 7 and 8. The velocity profile in the channel became flatter and two velocity peaks, or the 'M' profile that is observed at the top of the channel, became prevalent.

A significant result is that the velocity profile was not as pronounced on the oxygen side of the cell, in comparison to the hydrogen side. This was partly due to the fact that only half the volume of oxygen was produced, which reduces the 'lift' effect on this side. In addition, the sphere of the oxygen bubble of influence can also be seen, as its greater size extends further into the bulk and flattens out its respective peak of the 'M' profile.

As a comparison, to the velocity profiles from two gas evolving electrodes, we can see in Figure 9 results from the electrolysis of the $NaCl/NaClO_3$ solution, where the cathode evolves gas at 100% efficiency, and the anode at only 2–4% efficiency. The $NaCl/NaClO_3$ electrolyte had slower relative velocities than the Na_2SO_4 solution, due mostly to the fact that there was only about half as much evolved gas providing the flow-inducing buoyancy.

4.3. *Relative velocity*

Particles of dust and other contaminants, far smaller in size than the bubbles, were also present in the solutions. LDV could use these to calculate the liquid velocity, and if it was different to the bubble velocity, then a slip velocity would exist. The results showed that there were no slip velocities and the following derivation tests the validity of this conclusion. Liquid velocity in the bubble layer can be calculated by using the relative velocity model defined by Vogt [1]:

$$U_r = U_\infty(1 - \beta)^n \tag{1}$$

where U_∞ is the velocity of a single bubble in a quiescent flow and n is a coefficient depending on β, which is the volumetric flow gas fraction, where

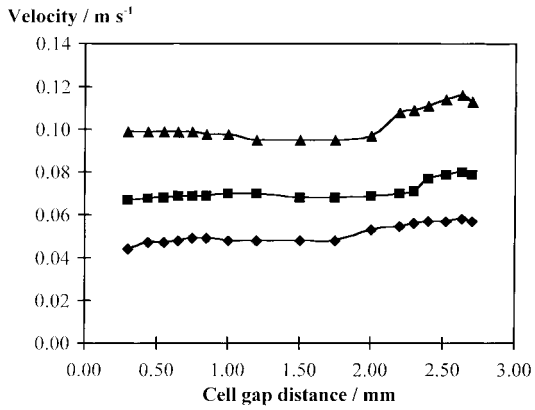

Fig. 7. Velocity profiles at the top of the electrodes, position 3, for the three current densities: $j = 500$ (◆), 1000 (■), 2000 (▲) A m^{-2}, in a Na_2SO_4 (50 g l^{-1}) electrolyte.

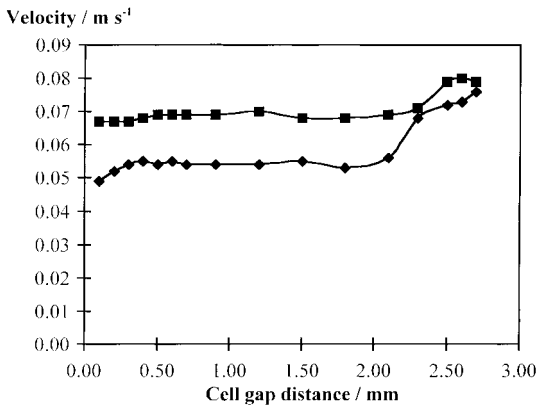

Fig. 9. The effect of oxygen bubble evolution, at the anode, has on the velocity profiles in the channel at position 3, for $j = 1000$ A m^{-2} in a NaCl (50 g l^{-1})/$NaClO_3$ (200 g l^{-1}) electrolyte (◆) and in a Na_2SO_4 (50 g l^{-1}) electrolyte (■).

$$\beta = \frac{Q_g}{Q_g + Q_l} \tag{2}$$

U_r is the relative velocity between bubble and liquid flow and is described by

$$U_r = U_b - U_l \tag{3}$$

Faraday's Law gives gas fractions no greater than 4%, at the current density values used in the experiments, which are less than the 30% specified by Vogt [20]. This allows us to set n as equalling 4. U_∞ is constant for all bubbles in the range of 50–100 μm and, in the present case, where the bubble Reynolds number is less than 1.4, $U_\infty = 5 \times 10^{-3}$ m s^{-1}. Combining Equations 1, 2 and 3 gives

$$U_l = U_b - U_\infty \left(1 - \frac{Q_g}{Q_g + Q_l}\right)^4 \tag{4}$$

Table 1 summarizes U_l, calculated from the equation, at each current density across the first 0.55 mm of the channel, at position 3 in the cell. As LDV uses light scattered from the bubbles to calculate velocity, the experimental values in Figures 6–9 represent the bubble velocity. Table 1 also shows the difference between calculated liquid velocity and the experimental bubble velocity, as U_r, along with the relative size of this difference.

The maximum relative difference was 7%, which falls into the region of experimental error, and subsequently leads to the conclusion that the two-phase flow can basically be considered as a homogeneous fluid. Our results are in good agreement with the literature, which says that relative velocity is very low in gas evolving systems of small gas fractions [20]. This is explained by the fact that two-phase flow in a channel of finite dimensions and at conditions of continuity develops a relative counter-flow of liquid somewhere in the channel, globally braking or hindering the slip velocity of the bubble [15]. In addition, the momentum transport caused by groups of bubbles rising together creates a velocity to which the bubbles and surrounding liquid generally adhere.

Table 1. Liquid velocities, U_l, in the bubble layer at positions 3, as calculated by Equation 4, for the three current densities: $j = 500$, 1000, 2000 A m^{-2}
The graph compares the difference between measured velocities, at position 3 (Figure 7), with those calculated

y/mm	j/A m^{-2}	U_l/m s^{-1}	U_r/m s^{-1}	U_r/U_b
0.3	500	0.053	0.004	0.07
0.4	500	0.054	0.004	0.07
0.52	500	0.053	0.004	0.07
0.3	1000	0.074	0.005	0.06
0.4	1000	0.075	0.005	0.06
0.52	1000	0.074	0.005	0.06
0.3	2000	0.111	0.005	0.04
0.4	2000	0.109	0.005	0.04
0.55	2000	0.106	0.005	0.04

4.4. *Velocity fluctuations and transition to turbulence*

In an individual experiment, a flat-plate cathode placed in the Na_2SO_4 solution was run at a current density of 1000 A m^{-2}, where the anode was placed in the bath so it could not interfere with the resultant two-phase flow. At the bottom of the electrode, bubbles were aligned and followed parallel stream lines until fluctuations began to develop. This showed that there existed a transition from laminar to turbulent behaviour, up the length of a planar surface that evolved bubbles. It was thought that the same behaviour could exist when the anode was present and formed a channel, so that this phenomenon would depend only on current density and cell height.

LDV can measure velocity fluctuations and give the root mean square (RMS) of this signal as the following:

$$\text{RMS} = \sqrt{\bar{u}'^2} \tag{5}$$

where $\bar{u}'$ is the fluctuating velocity of U_l [35]. The fluctuating velocity is a measure of the extent of deviations occurring from the mean velocity of a flow. The fluid mechanics quantity, turbulent intensity, is a statistical quantification of these deviations, and therefore provides a description of the extent of turbulence [35]. The RMS of the velocity fluctuations was measured at all four positions in the bubble layer, for the three current densities: $j = 500$, 1000 and 2000 A m^{-2}, and in the centre of the channel at $j = 1000$ A m^{-2}. It was then normalized by the mean velocity in the channel to give us the turbulent intensity, in the gas bubble layer, shown in Figure 10.

Results are compared to Boissonneau [33, 36] where turbulent intensity measurements were carried out in a

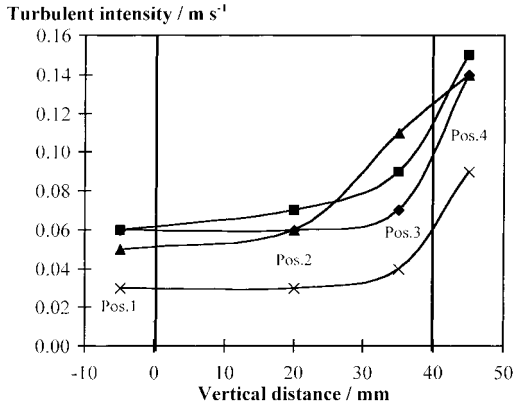

Fig. 10. Turbulent intensity evolution, in the bubble layer, along the length of the cathode for three current densities: $j = 500$ (◆), 1000 (■), 2000 (▲) A m^{-2} in an Na_2SO_4 (50 g l^{-1}) solution. Turbulent intensity in the centre of the channel, for $j = 1000$ A m^{-2}, is also given (×), and solid vertical lines indicate the placement of the entrance and exit to the cell channel.

two-phase flow, turbulent boundary layer, with a gas fraction of the order of 1×10^{-3}. In these experiments, turbulence intensity was found to be around 10% in the logarithmic part of the turbulent boundary layer. Lance et al. [37] ran a process where isotropic turbulence was imposed onto a two-phase flow, with a 3% gas fraction, and turbulent intensity was in the range from 10 to 12%. Therefore, at positions 3 and 4, where turbulent intensity is in the range from 10 to 15%, flow is turbulent for the cases of the highest current densities of 1000 A m^{-2} and 2000 A m^{-2}. At position 1, turbulence intensity is around 5% for all three of the current densities, meaning that the flow is laminar below the electrodes.

Transition between laminar and turbulent flows occurs at different locations along the cathode lengths, depending on the respective current densities. For the greater current density values, transition appears to occur between positions 2 and 3, while it does so after position 3 for the case of 500 A m^{-2}. Turbulent intensity development in the centre of the channel was far less than that in the bubble layer. This means that due to the lack of bubbles, the flow in the centre of the channel was laminar and that it only began to be turbulent towards the top of the channel. It also means that both turbulent and laminar properties in the fluid can exist at the same horizontal plane.

4.5. *PIV visualisation and transition to turbulence*

To locate the exact point of transition from laminar to turbulent flow, images of the flow in the channel were taken using PIV, which gives instantaneous global views of the bubble layer behaviour along the cathode. The total vertical length of the electrodes could not be seen at the one time so that shots were taken at four positions, segmenting the electrodes in four equal lengths, in order to follow the flow development in the channel. We have, therefore, assumed that we have a steady-state flow where transition to turbulence occurs at the same position irrespective of the time variable.

Measurements were carried out for $j = 1000$ A m^{-2} as shown in Figure 11. Slow expansion of the bubble layer thickness occurs up the length of the cathode, and the flow is laminar in the first two images, as the bubbles stay aligned and the scattered light has the same intensity throughout the bubble layer. The image of the bubble layer changes in the third centimetre, where large localised bubble bursts appear in the middle of the third image. In the fourth image, the transition has occurred as waves to the bubble layer become noticeable, an indication of it breaking up. The same basic behaviour was observed for the other current densities, although the waves appeared above the electrodes in the case of $j = 500$ A m^{-2}. It is too difficult to say exactly where transition ends and turbulence starts, although the results basically show that turbulence does occur up the length of the electrode. Unfortunately, it was too difficult for PIV to resolve and analyse the velocity vectors.

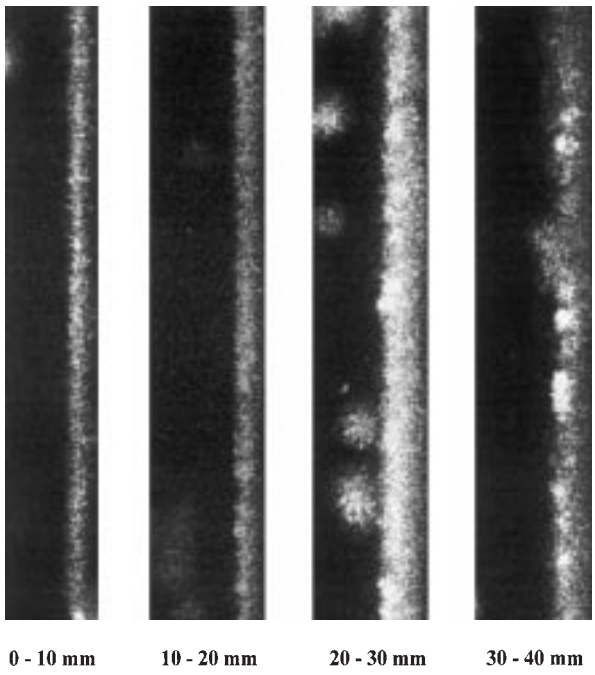

Fig. 11. Bubble layer and flow development up the length of the cathode, in 10 mm intervals, from the bottom to the top. Images taken with PIV at the cathode with $j = 1000$ A m^{-2} in a Na_2SO_4 (50 g l^{-1}) solution.

4.6. *Comparison of the measurement methods*

A comparison between the three measuring methods indicates that LDV is far more useful than the other two methods in investigating the hydrodynamics of gas-evolving systems. Visualization through magnification is useful for achieving a qualitative picture of what is occurring in the system, and the size range of the bubbles. PIV is also only good for a qualitative picture of the system. LDV has given some good results, and seems able to handle systems with small bubbles when they are not too concentrated. LDV could measure the bubble velocity vectors as well as being able to discern where the bubble diffusion layer existed. The method was not good at studying either the hydrodynamics or the bubbles themselves, both at the electrode surface and in the bubble adherence layer. Other velocimetry treatments exist and it is possible that some of them are more suitable for systems with bubbles.

Acknowledgements

The authors acknowledge the helpfulness and advice of Johan Persson of Vattenfall Utveckling AB, Älvkarleby, and Anders Dahlkild, Daniel Söderberg and Nils Tillmark of The Faxen Laboratory, all in Sweden. Permascand AB, Ljungaverk, Sweden, is also acknowledged for providing the electrochemical cell.

References

1. H. Vogt, *in* B.E. Conway, J.O′M. Bockris, E. Yeager, S.U.M. Khan and R.E. White (eds) 'Comprehensive Treatise of Electrochemistry', Vol. 6 (Plenum Press, New York, 1983), pp. 445–489.
2. Ph. Byrne, D. Simonsson, E. Fontes and D. Lucor, *in* A. Alemany, Ph. Marty and J.P. Thibault (eds) 'Fluid Mechanics and its Applications', Vol. 51: 'Transfer Phenomena in Magnetohydrodynamic and Electroconducting Flows' (Kluwer Academic, Dordrecht, The Netherlands, 1999), pp. 137–152.
3. N. Ibl and D. Landolt, *J. Electrochem. Soc.* **115** (1968) 713.
4. A.R. Despic, M.M. Jaksic and B.Z. Nikolic, *J. Appl. Electrochem.* **2** (1972) 337.
5. S.G. Bankoff, ASME, *J. Heat Transfer* **82** (1960) 265.
6. N. Zuber and J.A. Finlay, *J. Heat Transfer* **87** (1965) 453.
7. G.B. Wallis, Paper no. 38, ASME, *International Heat Transfer Conference*, Boulder, CO., **2** (1961) 319.
8. S.W. Beyerlein, R.K. Cossmann and H.J. Ritcher, *Int. J. Multiphase Flow* **11** (1985) 629.
9. N. Clark and N. Flemmer, *Int. J. Multiphase Flow* **12** (1986) 299.
10. M. Sadatomi and Y. Sato, *Int. J. Multiphase Flow* **8** (1982) 641.
11. H. Vogt, *Electrochim. Acta* **29** (1984) 167.
12. H. Vogt, *Electrochim. Acta* **29** (1984) 175.
13. R.R. Lessard and A.S. Zieminski, *Ind. Eng. Chem. Fundam.* **10** (1971) 260.
14. G. Marrucci and L. Nicodemo, *Chem. Eng. Sci.* **22** (1967) 1257.
15. J.P. Prince and H.W. Blanch, *AI Chem. Eng. J.* **36** (1990) 1485.
16. L.J.J. Janssen, *Electrochim. Acta* **34** (1989) 161.
17. J. Venczel, PhD thesis, ETH, Zurich, Prom no. 3673 (1961).
18. S.J.D. Van Strallen and W.M. Sluyter, *J. Appl. Electrochem.* **15** (1985) 527.
19. H. Vogt, *Electrochim. Acta* **34** (1989) 1429.
20. H. Vogt, *Electrochim. Acta* **26** (1981) 1311.
21. J.P. Glas and J.W. Westwater, *Int. J. Heat Mass Transf.* **7** (1964) 1427.
22. D. Landolt, R. Acosta, R.H. Muller and C.W. Tobias, *J. Electrochem. Soc.* **117** (1970) 839.
23. L.J.J. Janssen, *Electrochim. Acta* **23** (1978) 81.
24. N. Ibl, E. Adam, J. Venczel and E. Schalch, *Chem. Ing. Tech.* **43** (1971) 202.
25. H. Vogt, 'Ein Beitrag zum Stoffubergang an gasentwickelnden Elelktroden', PhD thesis, University of Stuttgart, Germany (1977).
26. L.J.J. Janssen and J.G. Hoogland, *Electrochim. Acta* **15** (1970) 1013.
27. Y. Fukunaka, K. Suzuki, A. Ueda and Y. Kondo, *J. Electrochem. Soc.* **136** (1989) 1002.
28. D. Ziegler and J.W. Evans, *J. Electrochim. Soc.* **133** (1986) 567.
29. F. Hine, M. Yasuda, R. Nakaruma and T. Noda, *J. Electrochim. Soc.* **122** (1975) 1185.
30. J.M. Bisang, *J. Appl. Electrochem.* **21** (1991) 760.
31. L.J.J. Janssen and G.J. Visser, *J. Appl. Electrochim.* **21** (1991) 386 and 753.
32. Y. Nishiki, K. Aoki, K. Tokuda and H. Matsuda, *J. Appl. Electrochim.* **16** (1986) 615.
33. P. Boissonneau, 'Propulsion MHD en eau de mer: étude des couplages hydrodynamique–électrochimie–électromagnetisme.' PhD thesis, UJF, Grenoble, France (1997).
34. F. Durst, A. Melling and J.H. Withlaw, 'Principles and Practice of Laser Doppler Anemometry' (Academic Press, London, 1976).
35. H. Schlichting, 'Boundary Layer Theory, 4th edn (McGraw-Hill, New York, 1960).
36. P. Boissonneau and J.P. Thibault, *in* A. Alemany, Ph. Marty and J.P. Thibault (eds) 'Fluid Mechanics and its Applications', Vol. 51: 'Transfer Phenomena in Magnetohydrodynamic and Electroconducting Flows' (Kluwer Academic, Dordrecht, The Netherlands, 1999), pp. 251–268.
37. M. Lance and Bataille, *Int. J. Fluid Mech.* **222** (1991) 95.